J. Phys. B: At. Mol. Opt. Phys. **25** (1992) 3505-3512. Printed in the UK

Cusp electron emission in 1.4 MeV u^{-1} Xe^{26+} on Ar collisions as a function of the projectile final charge state

C F Chou†, R Koch‡, Y C Chang†, C C Hsu†, C Kelbch‡ and H Schmidt-Böcking‡

† Institut für Kernphysik, Johann Wolfgang Goethe-Universität 6000 Frankfurt/Main, Federal Republic of Germany

‡ Department of Physics, National Tsing Hua University, Hsinchu, Taiwan

Received 4 November 1991, in final form 24 February 1992

Abstract. The cusp electron emission as a function of the final projectile charge state has been investigated by an electron-projectile coincidence technique in 1.4 MeV u^{-1} Xe^{26+} on Ar collisions. The cusp electron emission production probability varies strongly with the final projectile charge state. It is highest for projectile electron loss processes, increases for capture processes with the number of electrons captured by the projectile and is lowest in the pure ionization channel. The observed results can be qualitatively explained by the different impact parameter dependencies of capture, loss and ionization processes with respect to cusp formation.

1. Introduction

The spectroscopy of cusp electrons has attracted great experimental and theoretical interest (Macek 1970, Breinig *et al* 1982, Menendez *et al* 1990) in order to improve the understanding of electron capture processes in ion-atom collisions. Cusp electrons are electrons in low-lying projectile continuum states which have a very small momentum in the projectile rest frame. Therefore, their emission probability at 0° emission angle is peaked around the energy $E_{cusp} \approx \frac{1}{2} m_e v_P$, which corresponds to electrons moving with the projectile velocity v_P. The width and shape of this 'cusp' contains detailed information about the initial electron momentum distribution and the production mechanisms. Two primary processes are mainly responsible for the production of cusp electrons, target-electron capture to the continuum (ECC) or projectile-electron loss to the continuum (ELC). ECC requires a mean momentum transfer to the target electron of $\Delta p_e \approx m_e v_P$, whereas for ELC the momentum transfer is $\Delta p_e \approx m_e v_{e,i}$. The mean velocity $v_{e,i}$ of the projectile electron in its initial state depends on the initial projectile charge state. Thus, cusp electron spectroscopy is dependent on the projectile velocity, the nuclear and ionic charge of the target and the projectile, allowing a sensitive test of electron capture and ionization theories, because of the known momentum transfers. While numerous investigations for lighter ions have been made (Andersen *et al* 1986, Jagutzki *et al* 1991, Köver *et al* 1989, Sarkadi *et al* 1989), only a small number of investigations for heavy ion-atom collisions have been reported in the literature (Andersen *et al* 1984, Datz *et al* 1990, Skutlartz *et al* 1988). It was found that the cusp electron production probability as a function of the projectile final charge state is strongly enhanced if another electron is captured into a bound state simultaneously. The simultaneous capture of two or more electrons might help to improve the matching

0953-4075/92/163505+08$04.50

conditions by electron–electron momentum exchange for the needed momentum transfer $m_e v_P$. The measurements of the impact parameter dependence of the cusp production in F^{8+}–Ne collisions as a function of the projectile final charge state show this correlation effect clearly (Skutlartz *et al* 1988).

Jagutzki *et al* (1991) derived from the comparison of their p, He^+ on He, Ne data with the F^{8+} on Ne data that this correlation effect might scale with a higher order of Z_p^α (where α was estimated to be about 6). For even more highly charged projectiles this correlation effect might become more dominant for the total cusp production and should show up in a strong variation of the total cusp cross-section with the final projectile charge state. However, such a variation can also accidentally be produced by a strong varying overlap in the impact parameter dependence of two uncorrelated processes: target electron ionization to high energetic continuum states near v_p as the first process; the second process is a subsequent post-collision capture of these electrons into low-lying projectile states.

Therefore, a large ECC cross-section for the capture channel could result from the fact that ECC mainly occurs in small impact parameter collisions where the projectile mostly undergoes a charge change process. The simultaneous multiple capture or loss to bound projectile states is thus an uncorrelated process and might have a similar impact parameter dependence as the δ-electron production for $v_\delta \approx v_P$. Reinhold *et al* have recently calculated this post-collision cusp formation in a CTMC approach and have found that it occurs at internuclear distances which are a few hundred times larger than the impact parameter (Reinhold and Olson 1989, Reinhold and Schultz 1989). Therefore, in agreement with the experimental findings of Jagutzki *et al* (1991), the cusp formation probability for uncorrelated processes is just the δ-electron production probability times the post-collision capture probability, which is nearly independent of the final projectile charge or should be larger for $n_f > n_i$ (loss) than for $n_f < n_i$ (capture). Measuring simultaneously the δ-electron and cusp formation probability of the final charge state for capture and loss one should be able to identify contributions from correlated e–e processes from the ratio of both probabilities as a function of the final charge state. To investigate a possible enhanced correlation effect in more highly charged projectiles $n_i > 20$ we measured the cusp and δ-electron production by means of electron–projectile coincidences in 1.4 MeV u^{-1} Xe^{26+} on Ar collisions as a function of the final projectile charge state both for capture and loss processes.

2. Experimental procedure

The experiment was performed at the UNILAC of GSI-Darmstadt. An energy and charge state analysed 1.4 MeV u^{-1} Xe^{26+} beam was well collimated to a spot of less than 1 mm^2 and intersected an Ar gas target. The pressure inside the gas cell of 15 mm diameter was 3×10^{-3} torr, measured and controlled by a capacitance manometer. The final projectile charge states were magnetically analysed and detected by a position-sensitive parallel-plate avalanche detector (PPAD). The electrons were measured under a 0° emission angle with respect to the beam direction and energy analysed in a 127° electrostatic cylindrical spectrometer, which was operated in scanning mode (see figure 1). It was located close behind the gas cell ($\approx$4 mm) such that the geometrical solid angle was approximately 0.2% of 4π. With an energy resolution of about 6% this ensures a large collection efficiency. The deflected electrons were finally detected with a channeltron device.

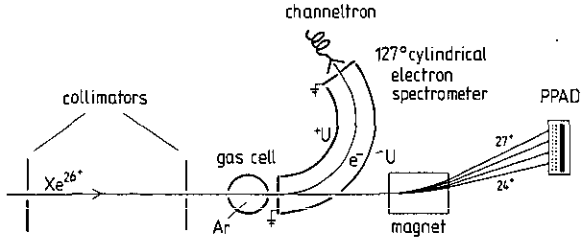

Figure 1. Sketch of the experimental set-up.

The vacuum chamber containing the gas target and the electron spectrometer was separated from the beamline by two apertures of 3 mm diameter. The beamline pressure was kept below 10^{-6} torr and the pressure inside the vacuum chamber never exceeded 8×10^{-6} torr. We measured the electron capture and loss rate of the projectiles as functions of the target pressure to ensure single-collision conditions. We found a linear relation for pressures up to 5×10^{-3} torr with an offset resulting from projectile charge exchange in the beamline. With a gas target pressure of 3×10^{-3} torr the ratio of projectile capture and loss processes produced in the target to those in the beamline was larger than five.

The *n*-pentane-filled PPAD ($P\approx10$ torr) consisted of two avalanche regions (see figure 2) and a wedge-and-strip anode to obtain position resolution. A 2 μm thick Mylar foil supported by a grid with high transmission (≈85%) was used as the entrance window. The incoming Xe ions produced sufficient ionization electrons in the first stage, which were accelerated by an electric field of $|E|\approx1000$ V cm^{-1} into the second stage. Here, secondary ionization amplified the number of primary electrons to about 10^8 per detected ion. This avalanche could be varied over a wide dynamic range by changing the electrostatic field between the two grids.

According the wedge-and-strip structure of the anode, the charge of the secondary ionization avalanche was geometrically divided into three fractions which were subsequently integrated by charge-sensitive preamplifiers. The position was calculated by charge division techniques on-line with the computer. With this electronic set-up, instantaneous count rates of 10^6 can be handled but during the experiment the average count rate had to be limited to about 3000 s^{-1} due to the pulsed UNILAC beam. In

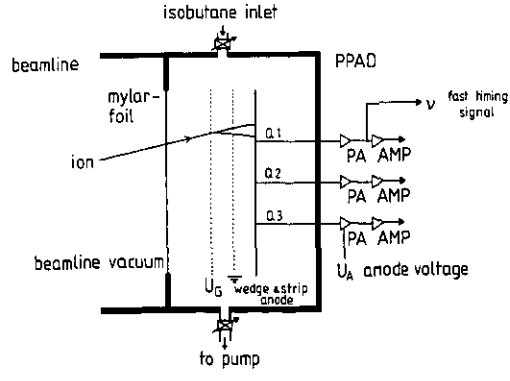

Figure 2. Schematic view of the parallel-plate avalanche detector (PPAD). Q1, Q2 and Q3 represent the collected charges of the three fractions of the wedge-and-strip anode.

figure 3 the measured time spectrum is displayed, showing the UNILAC micro time structure. It can be seen that the true coincidences could be well separated from the random coincidences. The coincidence data were stored event by event with a list mode data aquisition system based on an Atari ST computer with CAMAC interface (*Ullmann 1988*).

In figure 4 the electron spectra for the single-loss and single-capture channel are displayed. The horizontal bar indicates the experimental energy resolution. The cusp electron emission probabilities $P_{cusp}(n, n')$ as a function of the projectile final charge state (n') are

$$P_{cusp}(n, n') = \Delta N_{cusp}(n, n') 4\pi\varepsilon_e S(E_e)/N_p(n, n')/\Delta\Omega_e \qquad (1)$$

where ε_e denotes the channeltron detection efficiency, $S(E_e)$ the spectrometer scanning factor and $\Delta\Omega_e$ the geometric solid angle.

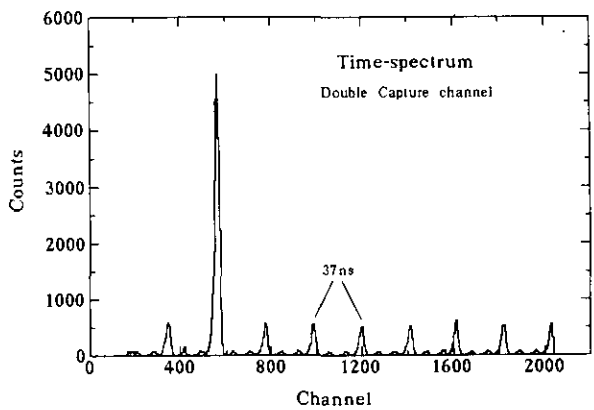

Figure 3. Time spectrum (double-capture channel) where the pulsed UNILAC beam structure of 27 MHz can be seen.

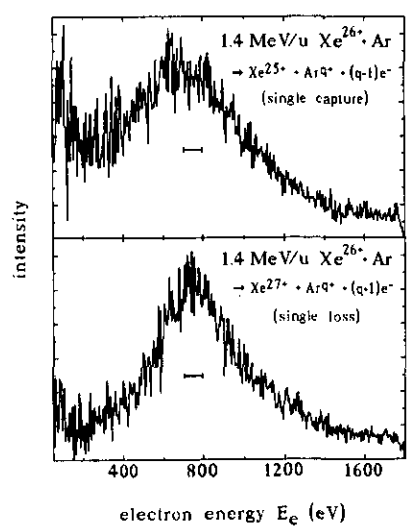

Figure 4. Coincident electron spectrum for single-electron loss and capture of the projectile.

The number of true coincidences in the cusp peak $\Delta N_{\text{cusp}}(n, n')$ was obtained by setting appropriate windows on the electron energies and the coincidence time. The δ-electron 'background' below the cusp and the random coincidences below the time peak were subtracted by extrapolation of the measured δ-electron contribution on both sides of the cusp peak into the region below the cusp peak. The statistical errors in the data were always of the order of 1-2% because of the high coincidence rates. The number $N_p(n, n')$ of detected particles in each charge state n' was directly counted by fast scalers and corrected for computer dead time. The remaining product,

$$g = \varepsilon_e S(E_e) 4\pi / \Delta\Omega_e \tag{2}$$

could not be measured accurately. $\Delta\Omega_e$ was not determined, because for cusp electron emission its value could only be estimated to be of the order of 40-50% of the total 4π solid angle. However, since the product g should be independent of n', only the relative $P^{\text{rel}}_{\text{cusp}}(n, n') = P_{\text{cusp}}(n, n')/g$ are shown and discussed.

Because the relative charge state fractions $f(n, n')$ of the outgoing Xe beam were measured simultaneously by the position-sensitive PPAD, the relative total cross-section $\sigma^{\text{rel}}_{\text{cusp}}(n, n')$ for cusp production could be derived as a function of the final charge state with

$$\sigma^{\text{rel}}_{\text{cusp}}(n, n') \approx P^{\text{rel}}_{\text{cusp}}(n, n')\sigma(n, n') \tag{3}$$

where $\sigma(n, n')$ are the corresponding cross-sections for charge changing collisions ($n = n'$ indicates pure target ionization without change of the projectile charge state, $n' = n+1$ single loss, $n' = n-1$ single capture, etc.).

3. Data and discussion

In figure 5 the relative cusp production cross-sections $\sigma^{\text{rel}}_{\text{cusp}}(n, n')$ are shown. The ionization channel is clearly dominating the total cusp production whereas the single loss is strongly suppressed in comparison to the capture channels. However, these data give only little information on the importance of the cusp production mechanisms, since these cross-sections are strongly influenced by the impact parameter dependence of pure ionization, capture and loss. Pure ionization occurs mainly at large impact parameters, where capture and loss have negligible probabilities. Because of the huge

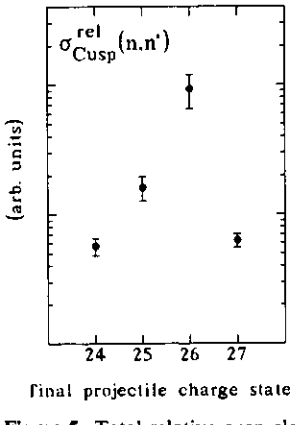

Figure 5. Total relative cusp electron cross-sections.

total ionization cross-section $\sigma^{tot}(n'=n) \geq 5\times10^{-14}$ cm^2 (Olson and Dörner 1990), we obtain that even for small cusp formation probabilities about 78% of all cusp electrons are produced in pure ionization events. The capture channels contribute with 17% and the loss channel only with about 5%.

To obtain more detailed information on the importance of the cusp production mechanisms we have to discuss the measured cusp production probabilities per ionization, capture and loss event. In figure 6 the relative cusp probabilities $P^{rel}_{cusp}(n, n')$ and those for the nearby δ-electron emission $P^{rel}_{\delta}(n, n')$ are displayed. For the single-electron loss channel we measured the highest cusp production probability, which clearly shows the importance of projectile ionization by the target Coulomb force to low-lying continuum states. From figure 4 we can derive that the loss contribution has a narrower cusp shape than the ECC distribution, as expected for the two mechanisms. P^{rel}_{cusp} for single capture is about four times lower compared to single loss; however, for double capture it increases again by a factor of two.

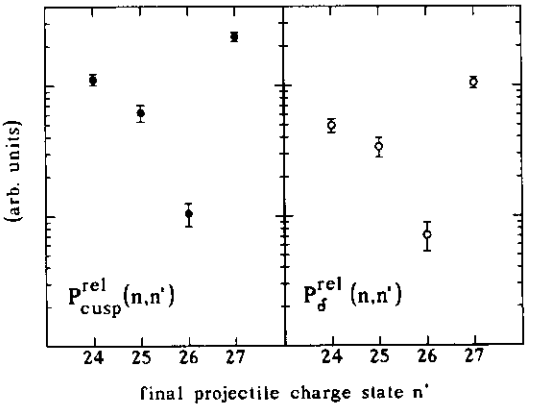

Figure 6. Relative cusp and δ-electron emission probabilities as functions of the final projectile charge state.

The data in figure 6 show that for pure ionization $P^{rel}_{cusp}(n'=n)$ is much smaller than for loss or capture events. This is expected, since for large impact parameter collisions, target electron capture in low-lying projectile continuum states is rather unlikely because of the required large momentum transfer $\Delta p_e \approx m_e v_P$. The large $P^{rel}_{cusp}(n'<n)$ values for capture channels can qualitatively be explained using the impact parameter picture: electron capture by the projectile occurs mainly at small impact parameters where momentum transfer to target electrons of $\Delta p_e \approx m_e v_P$ is much more likely than at large impact parameters. Also, the increase of P^{rel}_{cusp} from single to double capture by a factor of two can be explained in this framework. Double capture occurs in this collision system at even smaller b, where the probability for the momentum transfer of $m_e v_P$ is enhanced. Thus, we can conclude that the main features of P^{rel}_{cusp} as a function of n' can be explained by the different impact parameter dependencies of the different reaction channels and their overlap with the b-dependence of the uncorrelated cusp formation.

A detailed look, however, into the relative ratio between P^{rel}_{cusp} to the δ-electron emission probability as a function of n' shows (figure 7) that cusp formation accompanied by capture into bound states is not such an uncorrelated two-step process of

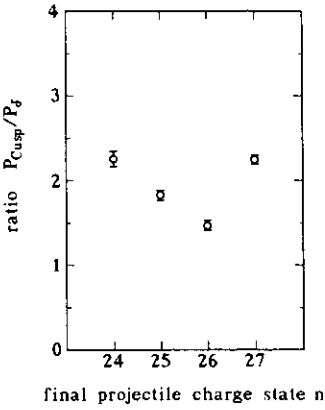

Figure 7. Ratio of cusp and δ-electron emission probabilities as functions of the final projectile charge state.

target ionization with final ejected electron momentum $m_e v_P$ and a post-collision 'focusing' into the cusp peak by the projectile Coulomb force. It was predicted by Reinhold and Olson (1989) that for the p-He system this process should dominate. Jagutzki *et al* (1991) found for the p-He system that this two-step process could explain the measured b-dependence of cusp formation. For Xe^{26+} on Ar, however, we observe that the ratio of $P_{cusp}(n')/P_\delta(n')$ increases with the number of captured electrons. Since the post-collision focusing strength slightly decreases from $n'=26$ to $n'=24$, we could expect in the two-step formation mechanism that this ratio would be proportional to the post-collision projectile charge. The observed increase, however, indicates that the electron-electron correlation contributes up to about 50% to the total cusp formation in the capture channels. This observation is in qualitative agreement with the findings of Skutlartz *et al* (1988) for cusp formation in 10 MeV F^{8+} on Ne collisions.

The expected strong increase ($\approx Z_p^6$) of the cusp formation by electron-electron correlation derived from the F^{8+}-Ne and p-He data has not been observed in the investigated Xe^{26+}-Ar system. Figure 7 shows that the ratio of cusp electrons to δ-electrons is for double capture only twice as high as for pure ionization.

Higher differential measurements, e.g. the impact parameter-dependent cusp emission as a function of the final charge state, are needed to illustrate the multiple-electron transfer processes in more detail. In the collision system investigated here, however, the established techniques (detection of projectile angle in coincidences with 0° electrons) are no longer applicable because the relevant scattering angles are below the mrad regime. Only the recently developed recoil ion momentum spectroscopy (Ullrich *et al* 1991) in coincidence with 0° electron emission has the ability to obtain information on ion-atom collisions with even smaller scattering angles.

Acknowledgments

Two of us (CFC and YCC) want to thank the IKF for the support they obtained during their stay at Frankfurt University. This work was supported by GSI-Darmstadt the Bundesministerium für Forschung und Technologie and the Academica Sinica/Taiwan.

References

Andersen L H, Frost M, Hvelplund P and Knudsen H 1984 *J. Phys. B: At. Mol. Phys.* **17** 4701
Andersen L H, Jensen K E and Knudsen H 1986 *J. Phys. B: At. Mol. Phys.* **19** L161
Breinig M *et al* 1982 *Phys. Rev.* A **25** 3015
Datz S *et al* 1990 *Phys. Rev.* A **41** 3559
Jagutzki O, Koch R, Skutlartz A, Kelbch C and Schmidt-Böcking H 1991 *J. Phys. B: At. Mol. Opt. Phys.* **24** 993
Köver A, Sarkadi L, Palinkas J, Berenyi D, Szabo G, Vajnai T, Heil O, Groeneveld K O, Gibbons J and Sellin I A 1989 *J. Phys. B: At. Mol. Opt. Phys.* **22** 1595
Macek J 1970 *Phys. Rev.* A **1** 235
Menendez M G, Huetz A and Duncan M M 1990 *Proc. 4th Workshop on High Energy Ion-Atom Collision Processes (Debrecen, 1990)* (Lecture Notes in Physics **376**) ed D Berenyi and G Hock
Olson R E and Dörner R 1990 *n-CTMC calculations* Private communication
Reinhold C O and Olson R E 1989 *Phys. Rev.* A **39** 3861
Reinhold C O and Schultz D R 1989 *J. Phys. B: At. Mol. Opt. Phys.* **22** L565
Sarkadi L, Palinkas J, Köver A, Berenyi D and Vajnai T 1989 *Phys. Rev. Lett.* **62** 527
Skutlartz A, Hagmann S and Schmidt-Böcking H 1988 *J. Phys. B: At. Mol. Opt. Phys.* **21** 3609
Ullmann K 1988 *Diplom thesis* IKF Frankfurt (unpublished)
Ullrich J, Dörner R, Lencinas S, Jagutzki O, Schmidt-Böcking H and Buck U 1991 *Nucl. Instrum. Methods* B **61** 415